Tidal network ontogeny: Channel initiation and early development

Andrea D'Alpaos, Stefano Lanzoni, and Marco Marani

Dipartimento di Ingegneria Idraulica, Marittima Ambientale e Geotecnica and International Centre for Hydrology "Dino Tonini," Università di Padova, Padova, Italy

Sergio Fagherazzi

School of Computational Science and Information Technology, Florida State University, Tallahassee, Florida, USA

Andrea Rinaldo

Dipartimento di Ingegneria Idraulica, Marittima Ambientale e Geotecnica and International Centre for Hydrology "Dino Tonini," Università di Padova, Padova, Italy

[1]   The long-term morphological evolution of tidal landforms in response to physical and ecological forcings is a subject of great theoretical and practical importance. Toward the goal of a comprehensive theoretical framework suitable for large-scale, long-term applications, we set up a mathematical model of tidal channel network initiation and early development, which is assumed to act on timescales considerably shorter than those of other landscape-forming ecomorphodynamical processes of tidal systems. A hydrodynamic model capable of describing the key landforming features in small tidal embayments is coupled with a morphodynamic model which retains the description of the main physical processes responsible for tidal channel initiation and network ontogeny. The overall model is designed for the further direct inclusion of the chief ecomorphological mechanisms, e.g., related to vegetation dynamics. We assume that water surface elevation gradients provide key elements for the description of the processes that drive incision, in particular the exceedance of a stability (or maintenance) shear stress. The model describes tidal network initiation and its progressive headward extension within tidal flats through the carving of incised cross sections, where the local shear stress exceeds a predefined, possibly site-dependent threshold value. The model proves capable of providing complex network structures and of reproducing several observed characteristics of geomorphic relevance. In particular, the synthetic networks generated through the model meet distinctive network statistics as, among others, unchanneled length and area probability distributions.

Citation: D'Alpaos, A., S. Lanzoni, M. Marani, S. Fagherazzi, and A. Rinaldo (2005), Tidal network ontogeny: Channel initiation and early development, *J. Geophys. Res.*, *110*, F02001, doi:10.1029/2004JF000182.

1. Introduction

[2]   Tidal networks exert a fundamental control on hydrodynamic, sediment and nutrient exchanges within tidal environments, which are characterized by highly heterogeneous landscapes and physical and biological properties [e.g., *Adam*, 1990; *Perillo*, 1995; *Allen*, 2000; *Friedrichs and Perry*, 2001] (see, e.g., Figure 1). To address issues of conservation of tidal environments, exposed to the effects of climate changes and often to increasing human pressure, it is therefore of critical importance to improve our understanding of the origins of tidal networks and their ontogeny and evolution.

[3]   Tidal embayments can be divided, from a structural point of view, into three main morphological domains, each characterized by different hydrodynamics and ecology: the salt marshes, the tidal flats and the channel network. Salt marshes, relatively more elevated areas of the tidal basin, are generally the byproduct of a complex erosional and depositional history. They are regularly flooded by the tide and colonized by halophytic vegetation, that is, vegetation that has adapted, to varying degrees, to salty and oxygen-poor environments. Salt marshes define the transition between permanently emerged and submerged environments, and thus the associated ecological gradients make them the subject of great ecological interest. Tidal flats are characterized by lower elevations, which do not allow their colonization by halophytic plants, and generally lie between the salt marshes and the deeper tidal basin. The third environment is represented by the channel network that
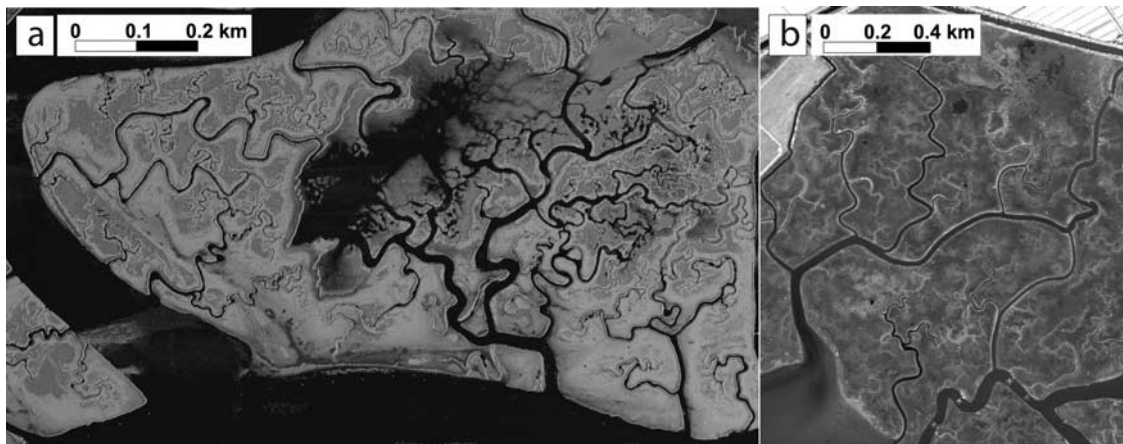
Figure 1. Two sample aerial photographs of field sites located in the northern part of the Venice Lagoon. Note the complexity of the tidal patterns and the variety of landforms characterizing such areas: (a) lidar image of the San Felice salt marsh; (b) aerial photograph of the Pagliaga salt marsh.

cuts through the tidal landscapes transporting flood and ebb discharges.

[4] A wide literature exists, developed especially in the last 2 decades, describing the hydrodynamics of tidal channels and creeks [e.g., *Boon*, 1975; *Pethick*, 1980; *Speer and Aubrey*, 1985; *Friedrichs and Aubrey*, 1988; *Lanzoni and Seminara*, 1998; *Savenije*, 2001; *Fagherazzi et al.*, 2003; *Lawrence et al.*, 2004], the consequences of tidal currents and asymmetries on sediment dynamics and other morphological characteristics of tidal channels [e.g., *Boon and Byrne*, 1981; *French and Stoddart*, 1992; *Friedrichs*, 1995; *Friedrichs et al.*, 1998; *Schuttelaars and de Swart*, 2000; *Lanzoni and Seminara*, 2002], morphometric analyses of tidal networks [e.g., *Myrick and Leopold*, 1963; *Pestrong*, 1965, 1972; *Leopold et al.*, 1993; *Steel and Pye*, 1997; *Fagherazzi et al.*, 1999; *Rinaldo et al.*, 1999a, 1999b; *Marani et al.*, 2002, 2003; *Di Silvio and Dal Monte*, 2003], sedimentation and accretion patterns in salt marshes [e.g., *Stoddart et al.*, 1989; *French and Spencer*, 1993; *Leonard and Luther*, 1995; *Ward et al.*, 1998; *Christiansen et al.*, 2000], ecological dynamics and patterns in salt marshes [e.g., *Yallop et al.*, 1994; *Marani et al.*, 2004; *Silvestri and Marani*, 2004]. Moreover, simplified models have also been proposed to simulate the morphological behavior of tidal basins [e.g., *van Dongeren and de Vriend*, 1994; *Schuttelaars and de Swart*, 1996] and to describe either the vertical movement of a marsh platform relative to a datum (zero-dimensional model) [e.g., *Beeftink*, 1966; *Pethick*, 1969; *Allen*, 1990, 1995; *French*, 1993; *Callaway et al.*, 1996; *Rybczyk et al.*, 1998], or such movement combined with the growth of the vertical sequence of underlying sediments (one-dimensional model) [e.g., *Allen*, 1995, 1997].

[5] Our efforts aim at using the large body of knowledge available on tidal environments to develop a model describing the long-term morphological evolution of a tidal system. Such a model should describe the planimetric development of tidal channel networks coupled with the vertical accretion of the adjacent salt marshes and tidal flats as a consequence of tidal forcings, varying sediment inputs and relative sea level changes. The mathematical modelling of tidal environment evolution requires the inclusion of several

ingredients related to the description of the delicate balance and strong feedbacks characterizing hydrodynamics, morphological and ecological dynamics. The joint actions of currents generated by tides, density gradients and wind, and the patterns of resuspension generated by waves govern the changes in the morphology of the tidal basin. These changes, in turn, have often a significant feedback on hydrodynamics and hence on the general tendency of the tidal embayment to import or export sediment. The evolution of topography in a tidal environment is the result of the balance between erosion and deposition of organic and inorganic soil and the vagaries of relative sea level. Sediment fluxes are not just controlled by the flow field but are also strongly influenced by the presence of halophytic vegetations and of microbial biofilms. Sediment transport processes may thus be seen as the byproduct of the complex interplay between hydrodynamics and ecology. External factors also matter, such as, among others, extreme storm events and changes in sediment supply associated with human interference. Thus one can conclude that coastal wetlands exist in a state resulting from the interaction of strong counteracting forces acting both in the horizontal and the vertical planes, leading either to their establishment and maintenance or to their rapid demolition. Chief landforming processes in the vertical plane are the combined actions of wind wave resuspension, compaction, subsidence and sea level rise, possibly compensated by accretion processes. Chief landforming processes in the horizontal plane are the early formation and the subsequent elaboration (e.g., by meandering) of the tidal channel network and erosion processes acting on the margins of salt marshes and tidal flats.

[6] In this paper, as a first step toward a complete model able to describe the long-term morphological evolution of a tidal system, we shall address the problem of channel network ontogeny and initial evolution over an existing tidal flat. As we shall discuss in section 3, the model imposes a null along-channel gradient in net sediment transport, and thereby a net balance of erosional and depositional processes, resulting in stable channeled shapes whose proxy is the local tidal prism, i.e., the total volume of water which is exchanged through the outlet of a channel

network between low water slack and the following high water slack, i.e., during flood or ebb. The model is strictly valid for relatively short tidal embayments so that a relatively fast propagation and a weak deformation of the tidal wave are ensured. The model further assumes that tidal meandering acts on timescales longer than those involved in network formation and does not include, at present, soil production processes nor any other morphodynamic interaction of physical, chemical and biological nature acting on timescales longer than those involved in the elaboration of the early tidal network.

[7] The paper is organized as follows. Section 2 discusses observational evidence, which will be used to develop and to test the model. In section 3 we introduce the physical assumptions and the mathematical structure of the model. Section 4 then presents and discusses the main results obtained by applying the model under different initial conditions. In this section we compare significant geomorphic features of the modelled networks to the ones of observed tidal patterns. Finally, section 5 deals with conclusions and some remarks on future developments.

2. Geomorphic Features of Tidal Networks: The Reference Framework

[8] The lack of scale-invariant landforms, consistently observed in the tidal environment, and the great diversity in geometrical and topological forms of tidal networks are suggested to stem from the strong spatial variability of landscape-forming flow rates, of sediment characteristics, of vegetation type and cover, and from competing dynamic processes acting at overlapping spatial scales.

[9] It should be emphasized here that our interest toward a synthesis of complex models is justified by the fact that a fully equipped model, solving the complete momentum and mass balance equations, could not conceivably be used for the mathematical description of the evolution of a tidal environment over morphologically meaningful periods of time. It has been shown, moreover, that a hydrodynamic Poisson-like mathematical model obtained by suitably simplifying the classical two-dimensional shallow water equations proves robust and reliable upon comparison with complete models in a large spectrum of cases of interest [*Rinaldo et al.*, 1999a; *Marani et al.*, 2003]. This bears important consequences, and calls for appropriate morphodynamic counterparts.

[10] One of the simplest geomorphic measures controlling tidal channel morphodynamic evolution is arguably the width-to-depth ratio $\beta = B/D$ [e.g., *Allen*, 2000; *Solari et al.*, 2002]. Variations in β values observed for tidal channels of different sizes within the Lagoon of Venice [*Marani et al.*, 2002] are consistent with the characteristics of different types of cross sections surveyed by *Allen* [2000] and with the great variability, and yet the consistent trends, obtained for the dependence of β on channel order by *Lawrence et al.* [2004]. This stems from the great diversity of the basic processes controlling the section shape. In particular, the presence on the marshes of halophytic vegetation and of relatively fine sediments, which are often cohesive, is likely to strongly affect bank failure mechanisms. As a consequence, salt marsh creeks and tidal flat channels are seen to respond to different erosional processes resulting in differ-

ent types of incisions. In fact, salt marsh creeks tend to be more deeply incised ($5 < \beta < 7$) than channels in tidal flats ($8 < \beta < 50$), where vegetation and generally sandier sediments are less likely to play a major role.

[11] The analysis of the geomorphic structure of channels, marshes and tidal flats allows important tests of geomorphic relationships relating measurable geometric or dynamic properties to landscape-forming flow rates. It has long been recognized that a power law relation between the tidal prism, P, and inlet minimum cross-sectional area, Ω, holds for a large number of tidal systems believed to have achieved dynamic equilibrium [*O'Brien*, 1969; *Jarrett*, 1976]. More recently, *Friedrichs* [1995], *Rinaldo et al.* [1999b] and *Lanzoni and Seminara* [2002] explored, in several tidal systems, the relationship between Ω and spring (i.e., maximum astronomical) peak discharge, Q. They found that a near proportionality between Ω and Q (which is directly related to the tidal prism) also exists for sheltered sections. Moreover this is in accordance with observations [e.g., *Myrick and Leopold*, 1963; *Nichols et al.*, 1991] suggesting a proportionality $\Omega \propto Q^{\alpha_q}$, with the scaling coefficient α_q in the range $0.85-1.20$. *Friedrichs* [1995] explains the existence of such relationship by relating the equilibrium cross-sectional geometry to the so-called stability shear stress, i.e., the total bottom shear stress just necessary to maintain a null along-channel gradient in net sediment transport. Well-defined power law relationships between channel width, cross-sectional area, watershed area and peak discharges were also documented [*van Dongeren and de Vriend*, 1994; *Fagherazzi et al.*, 1999; *Rinaldo et al.*, 1999a, 1999b], in accordance with morphometric analyses of tidal networks carried out by *Myrick and Leopold* [1963], and in analogy with fluvial networks [e.g., *Leopold et al.*, 1964]. In particular, it has been shown that an empirical relationship exists between channel cross-sectional area, Ω, and its drainage area, A, i.e., $\Omega \propto A^{\alpha_A}$, with $\alpha_A \sim 1$. It is thus an extension of Jarrett's "law" [*O'Brien*, 1969; *Jarrett*, 1976] in which we consider the cross-sectional area, Ω, to be related through a power law to the drainage area, A, computed according to the procedure outlined by *Rinaldo et al.* [1999a], instead of being related to the tidal prism, P, or the maximum peak discharge, Q. Indeed, substitution of drainage area for landforming discharge and the ensuing derivation of thresholds for erosional activities is an assumption usually adopted in landscape evolution theories [e.g., *Rinaldo et al.*, 1993, 1995; *Rigon et al.*, 1994] since it much simplifies models while retaining a clear physical link between morphological and dynamical properties of the system. We believe this to be relevant to the next generation of morphodynamic models, providing a simple means to approach complex spatial organizations of the parts and the whole.

[12] Comparisons to observed morphologies are performed in the framework of theoretical and observational analyses of the drainage density of tidal networks carried out by *Marani et al.* [2003], who provide the necessary geomorphic tools to test the reliability of synthetically generated networks. These analyses emphasize that the traditional Hortonian morphological description of the drainage density does not provide a distinctive picture of the geometry of a tidal network and of its relationship with the salt marsh it dissects. Indeed, site specific features of
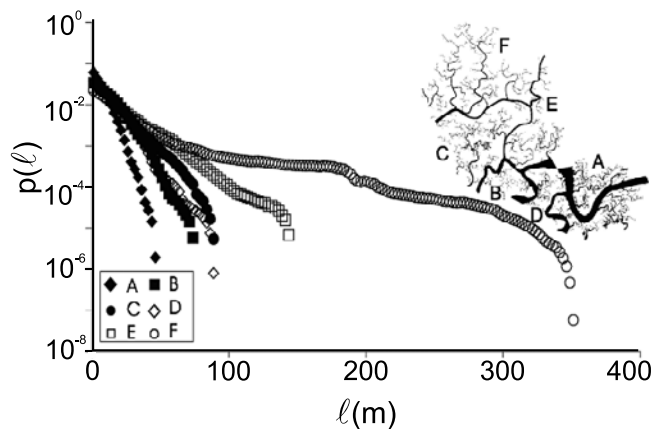
Figure 2. Probability density function of unchanneled flow length ℓ evaluated for several watersheds within the Pagliaga salt marsh. Note that an approximately straight observational trend on the semilog plot suggests an exponential distribution (adapted from *Marani et al.* [2003]).

network development and important morphological differences may only be captured by introducing measures of the extent of unchanneled flow lengths ℓ, whose determination requires the definition of suitable drainage directions defined by hydrodynamic, rather than topographic, gradients. For any unchanneled site defined within a tidal landscape we used the description of the hydrodynamic flow field and of its steepest descent directions (section 3.1) to determine the unchanneled flow path to the nearest tidal channel and to compute its length ℓ [*Marani et al.*, 2003]. Figure 2 shows the semilog plot of the probability density function of unchanneled flow lengths in different areas of the Pagliaga salt marsh, in the Venice lagoon (after *Marani et al.* [2003]). A clear tendency to develop watersheds described by exponential decays of the probability distributions of unchanneled lengths is observed, and thereby a pointed absence of scale-free features. Moreover such distributions are distinctive and allow us to distinguish significant network features such as different aggregation properties, subbasins shapes, branching and meandering.

[13] We shall also refer to global geomorphic measures like the distributions of total contributing area at a site, determined via the flow directions defined in the next section. As a note, we remark that we refrain from using topological measures like Strahler's orders, Horton's bifurcation and length ratios, Tokunaga's cyclicity for network comparison, because they are unable to identify differences between network structures [e.g., *Kirchner*, 1993; *Rinaldo and Rodríguez-Iturbe*, 1998].

3. Mathematical Model

[14] A mathematical model able to simulate the initiation and the early development of channel networks in tidal embayments, is set up by coupling the Poisson hydrodynamic model proposed by *Rinaldo et al.* [1999a] with a new morphodynamic model expressing channel network instantaneous adaptation to the hydrodynamic flow field characterizing the tidal basin at any stage of the evolution.

3.1. Hydrodynamic Field

[15] Before addressing the description of the morphodynamic model it is worthwhile to briefly recall the basic assumptions on which the simplified Poisson hydrodynamic model has been derived: (1) the tidal propagation across the intertidal areas flanking the channels is dominated by friction; (2) the spatial variations of the instantaneous water surface within the intertidal areas are significantly smaller than instantaneous average water depth, i.e., $\eta_1(\mathbf{x}, t) \ll \eta_0(t) - z_0$, where $\eta_1(\mathbf{x}, t)$ is the local deviation of water surface elevation from the instantaneous average tidal elevation, $\eta_0(t)$, and z_0 is the average bottom elevation (see Figure 3); (3) the fluctuations of unchanneled area bottom elevation around its mean, $z_1(\mathbf{x}) = z_b(\mathbf{x}) - z_0$, are significantly smaller than the instantaneous average water depth $\eta_0(t) - z_0$; (4) the propagation of a tidal wave within deep channels, where both inertia and resistance likely matter, is much faster than across the shallow, friction-dominated marsh platform. Hence we assume instantaneous propagation within the length of the tidal channels (here denoted by $\partial\Gamma''$), resulting in spatially independent local elevations $\eta_1 = 0$. This is in principle strictly valid only for relatively short tidal basins. Under these conditions, *Rinaldo et al.* [1999a] showed that, for a given instant t, the field of free surface elevations can be determined by solving the following Poisson boundary value problem:

$$
\begin{aligned}
\nabla^2 \eta_1 &= \frac{\lambda}{[\eta_0 - z_0]^2}\frac{\partial \eta_0}{\partial t} \qquad \text{within } \Gamma, \\
\frac{\partial \eta_1}{\partial n} &= 0 \qquad \text{on } \partial\Gamma', \qquad (1)\\
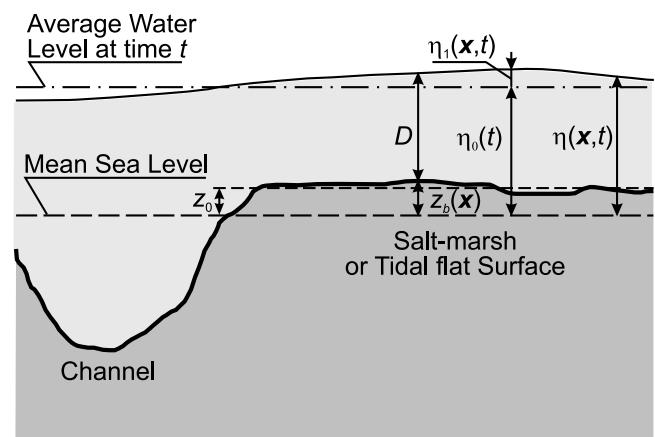\eta_1 &= 0 \qquad \text{on } \partial\Gamma'',
\end{aligned}
$$

Figure 3. Sketch of water elevation and bottom topography of a typical intertidal area. Notation used in the theory presented here is as follows: $\eta(\mathbf{x}, t) = \eta_0(t) + \eta_1(\mathbf{x}, t)$, instantaneous tidal elevation with respect to the mean sea level, where $\eta_0(t)$ is the instantaneous average tidal elevation within the intertidal areas at time t, referenced to the mean sea level; $\eta_1(\mathbf{x}, t)$, local deviation of water surface elevation from $\eta_0(t)$; D, instantaneous water depth on salt marsh or tidal flat surface; z_b, unchanneled area bottom elevation referenced to the mean sea level; z_0, average bottom elevation (adapted from *Rinaldo et al.* [1999a]).
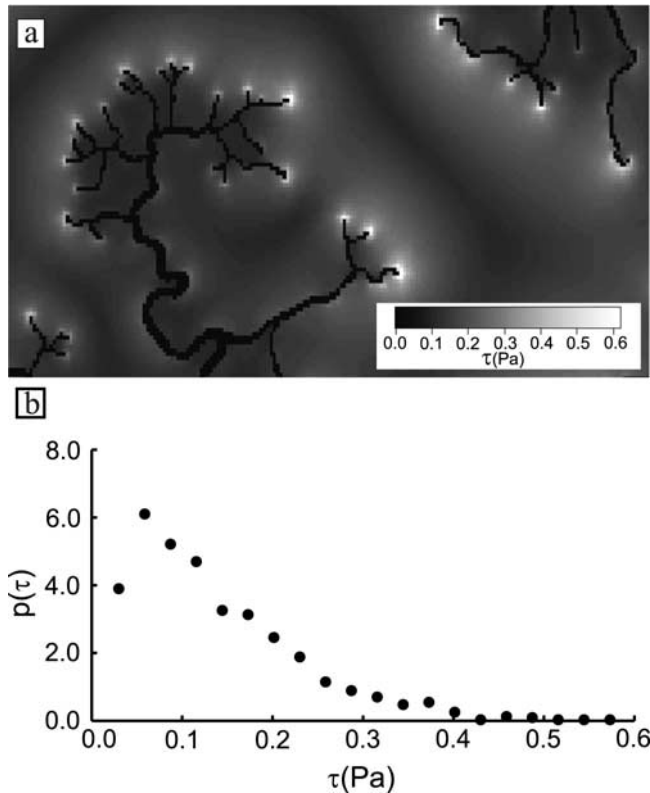
Figure 4. (a) Shear stress spatial distribution over unchanneled sites $\tau(\mathbf{x})$ and (b) probability density function $p(\tau)$ of bottom shear stress $\tau(\mathbf{x})$ computed in the neighborhood of channel tips of the tidal network developed within the Pagliaga salt marsh.

where Γ denotes the flow field domain, $\partial\Gamma'$ indicates impermeable boundaries on which we apply the requirement of zero flux in the direction n normal to the boundary, and $\partial\Gamma''$ denotes the channel network. The friction coefficient $\lambda = (8/3\pi)(U_0/\chi^2)$ in equation (1), which depends on Chèzy's friction coefficient χ and on a characteristic value of the maximum tidal current U_0, is taken to be constant within the considered intertidal regions, while the time-dependent forcing term on the right-hand side of equation (1) has to be assigned. The latter is estimated at a given time using representative values of η_0 and $\partial\eta_0/\partial t$, once a forcing tide with period, amplitude and phase lag typical of spring conditions is defined [see, e.g., *Rinaldo et al.*, 1999b]. On the basis of the resulting time-independent water surface obtained by solving the Poisson boundary value problem in equation (1), flow directions can be obtained at any location on the intertidal areas by determining its steepest descent direction, i.e., the direction determined by $\nabla\eta_1(\mathbf{x})$. Watersheds related to any channel cross section may thus be identified by finding the set of pixels draining through that cross section. Stringent tests of the validity of the embedded approximations and of the robustness of the model were carried out by *Marani et al.* [2003] who relaxed assumption 4 and assumed the tidal elevation varied in space and in time within the channel network. Suffice it here to say that this procedure makes it possible to evaluate the time variability of watershed extent and the migration in time of the divides. In particular the

results of *Marani et al.* [2003] emphasize that the tendency toward a constant time-independent value of watershed areas [*Rinaldo et al.*, 1999a] is enhanced as the flow resistance over the intertidal regions increases (a common circumstance, e.g., due to the presence of dense vegetation), and as the water level is slightly above the average elevation of the flats, both in the rising and in the falling phases of the tide, when the maximum flood and ebb discharges are likely to occur. Moreover, a comparison between the values of the maximum discharges obtained through the simplified model and those obtained from a full-fledged finite element model of the complete equations, showed that the Poisson model simply coupled with continuity is indeed surprisingly robust [*Marani et al.*, 2003]. This validation suggests that the model may be applied to estimate watersheds and landforming discharges even when the hypothesis of a small tidal basin is not strictly met.

[16] From a morphological point of view it is worthwhile to point out that the spatial water surface distribution resulting from equation (1) makes it possible to evaluate the bottom shear stress $\tau(\mathbf{x})$ acting on intertidal areas. Indeed, assumptions 1, 2 and 3 of section 3.1 imply that a balance between water surface slope and friction holds in the momentum equations, which allows one to write

$$\left(\frac{\partial\eta_1}{\partial x}, \frac{\partial\eta_1}{\partial y}\right) = -\frac{1}{\gamma D}\left(\tau_x, \tau_y\right), \qquad (2)$$

where $(\partial\eta_1/\partial x, \partial\eta_1/\partial y)$ denote the water surface slope in the (x, y) directions, (τ_x, τ_y) are the local shear stress in the (x, y) directions, $D(= \eta_0 + \eta_1(\mathbf{x}) - z_b(\mathbf{x}))$ is the flow depth (Figure 3) and γ is the specific weight of water. Therefore the shear stress produced by the tidal flow on the unchanneled portions of the tidal basin reads

$$\tau(\mathbf{x}) = \gamma[\eta_0 + \eta_1(\mathbf{x}) - z_b(\mathbf{x})]|\nabla\eta_1(\mathbf{x})|, \qquad (3)$$

where $\nabla\eta_1(\mathbf{x})$ is the water surface local slope.

[17] Where do tidal channels begin (or end)? To answer this question, echoing landmarks in fluvial geomorphology [*Montgomery and Dietrich*, 1988], we have studied, through equation (3), the spatial distribution of the shear stress $\tau(\mathbf{x})$ in unchanneled areas from our study sites within the Venice lagoon. These results are valuable in suggesting features of possibly general interest.

[18] In Figure 4a we show an example of the spatial distribution of $\tau(\mathbf{x})$ from the Pagliaga salt marsh (see Figure 1). We observe that the local maxima of the bottom shear stress $\tau(\mathbf{x})$ are located near the tips of the channel network and near channel bends (Figure 4a). We thus support the notion that erosional activities can be primarily expected in those parts of the tidal basin where the local value of the hydrodynamic shear stress is maximum and exceeding a threshold value for erosion, τ_c. Figure 4b represents the probability density function of $\tau(\mathbf{x})$ values computed in the neighborhood of channel tips. Under the assumption of approximately stable network configurations, the observed probability distributions provide useful information on the critical shear stress values, which will be used in numerical simulations.
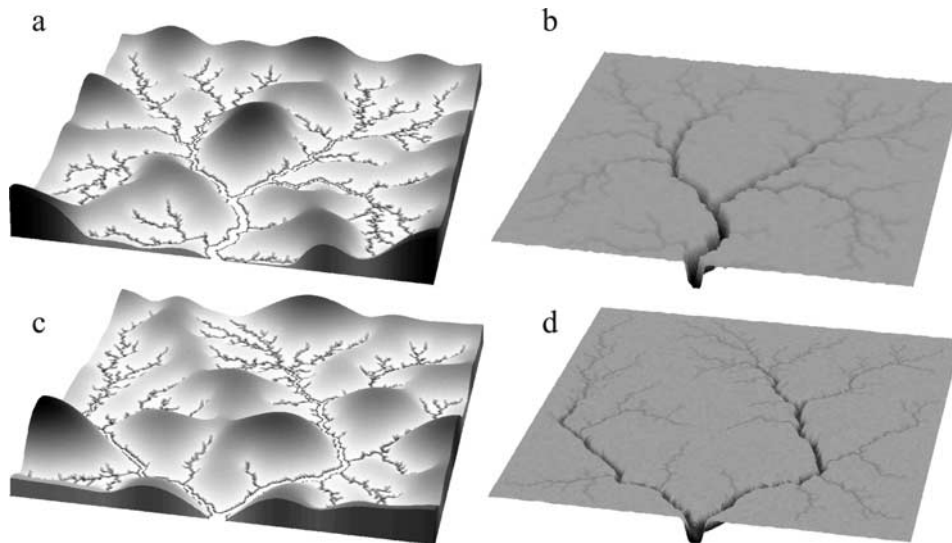
Figure 5. (a, c) Vertically exaggerated representation of the final water surface elevation field $\eta_1(\mathbf{x}) = \eta_1(\mathbf{x}, \infty)$ derived by solving equation (1) and (b, d) resulting carved topography $z_b(\mathbf{x}) = z_b(\mathbf{x}, \infty)$ for two experiments carried out in a square domain (to which a 256×256 lattice is superimposed) with no-flux boundary conditions applied on all basins' boundaries. A breach is opened on the lower boundary adjacent to the sea. We have obtained both simulations starting from the same initial hydrodynamic conditions: (1) $U_0 = 0.5$ ms^{-1}; (2) $\chi = 30$ m$^{1/2}$ s^{-1}; (3) $\eta_0 = 0.2$ m above mean sea level (amsl); $\partial\eta_0/\partial t = 8 \times 10^{-5}$ ms^{-1}; and (4) the same initial conditions for the field of bottom elevations $z_b(\mathbf{x}, 0) = z_0 + z_1(\mathbf{x})$ (i.e., $z_0 = 0$ m amsl and the uncorrelated Gaussian noise with mean $\langle z_1(\mathbf{x}) \rangle = 0$ and standard deviation $\sigma_{z_1(\mathbf{x})} = 0.02$ m). The size of the pixel is assumed to be equal to 1 m. Other values of the parameters are $\tau_c = 0.3$ Pa, $T = 0.3$ m, and $\alpha_A = 1.0$. We have carried out the first experiment (Figures 5a and 5b) by assuming a constant value of the width-to-depth ratio $\beta = 6$ and the second (Figures 5c and 5d) by assuming $\beta = 20$ if the drainage area to the generic channel cross section A is larger or equal to $A_{\text{tot}}/2$, where A_{tot} is the total catchment area, and $\beta = 6$ if A is smaller than $A_{\text{tot}}/2$, to account for observations by *Marani et al.* [2002]. See color version of this figure in the HTML.

[19] Note that the influence of such characteristics as the heterogeneity of vegetation, sediment sorting, marine transgressions and regressions on channel network dynamics can be tuned to appropriate variations of τ_c in space and time.

3.2. Morphodynamic Model

[20] Few systematic observations on rates of change in tidal channel geometry and network characteristics have so far been assembled which might be used to develop and test morphodynamic models [*Allen*, 2000]. However, observational evidence, e.g., time evolution of tidal networks analyzed from aerial photographs and field surveys, points at a rapid initial network formation. Such a quick initial network incision is later followed by elaboration that does not alter its major features and, possibly, by vertical accretion of intertidal areas which usually become vegetated when a critical bottom elevation is exceeded. Moreover this is in agreement with a number of conceptual models of salt marsh growth [e.g., *Beeftink*, 1966; *Pethick*, 1969; *French and Stoddart*, 1992; *French*, 1993; *Steel and Pye*, 1997; *Allen*, 1997]. These models support the hypothesis that a time in the life of a tidal network exists during which it quickly cuts down the intertidal areas giving them a permanent imprinting, in analogy with the case of fluvial settings [e.g., *Howard*, 1994; *Rodríguez-Iturbe and Rinaldo*, 1997]. Furthermore the spatial distribution of shear stresses, computed for several actual networks within the Venice lagoon (e.g., see Figure 4a), emphasizes that higher values of $\tau(\mathbf{x})$ are located near the initial incisions. This fact, together with the observed dynamics of first-order channels (documented to grow headward at rates up to many meters annually [e.g., *Pethick*, 1969]), strongly suggests that headward erosion is a major process in network development. Headward growth, driven by the spatial distribution of local bottom shear stress, and tributary initiation are thus here considered the main processes of channel network development during its earlier stages, leading to increasing network density and complexity. These considerations indicate the existence of different timescales governing the various processes and suggest the validity of the choice of decoupling the initial rapid incision of a tidal network from its subsequent slower process-controlled elaboration (chiefly by meandering) and from ecomorphological evolution of intertidal areas. This latter phase will be dealt with elsewhere. We do not support, based on the evidence we have collected and on the literature, the hypothesis of network formation through coalescence of unconnected channel "segments" separately originated and then joined together. Channel segmentation through local infilling caused by processes like bridging by overhanging vegetation or obstruction by collapsed silt blocks appears to be deemed of lesser importance [*Pestrong*, 1972; *Collins et al.*, 1987].
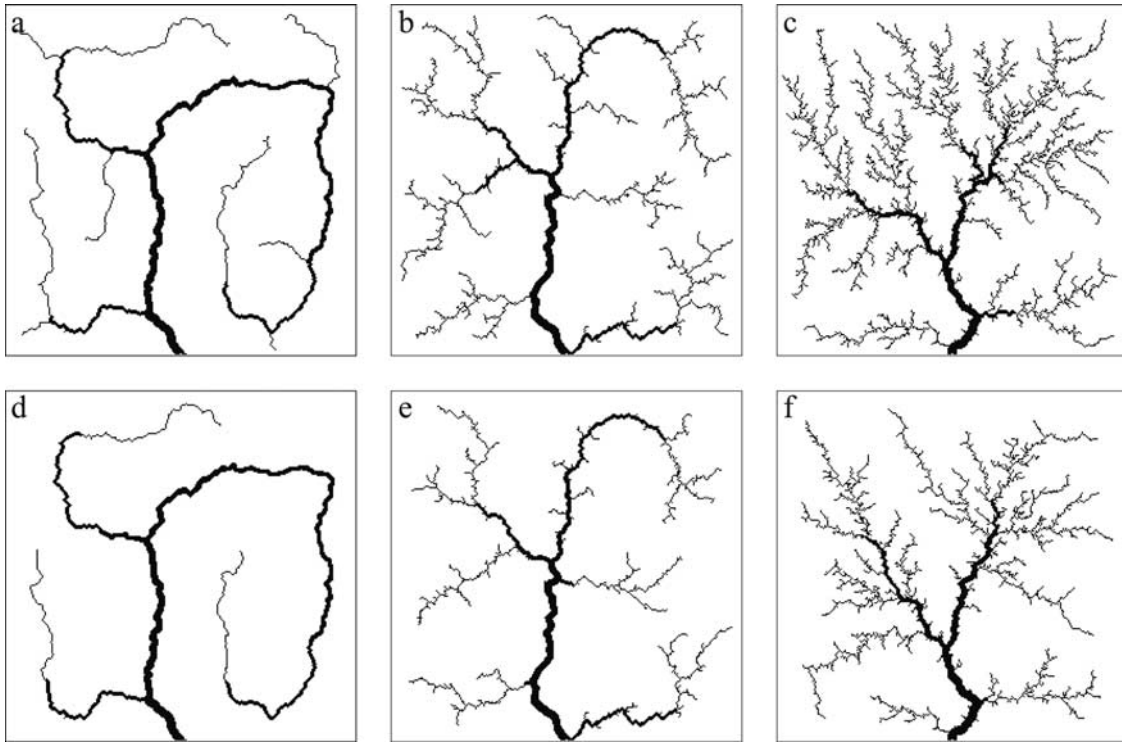
Figure 6. Sample of the effects of different values assigned to T and τ_c. The initial hydrodynamic conditions, the dimensions of the square basin, and the initial field of bottom elevations are the same as in Figure 5. Other values of the parameters are $\beta = 6$ and $\alpha_A = 1.0$. (a) $\tau_c = 0.3$ Pa, $T = 0.0001$ m; (b) $\tau_c = 0.3$ Pa, $T = 0.1$ m; (c) $\tau_c = 0.3$ Pa, $T = 1.0$ m; (d) $\tau_c = 0.5$ Pa, $T = 0.0001$ m; (e) $\tau_c = 0.5$ Pa, $T = 0.1$ m; (f) $\tau_c = 0.5$ Pa, $T = 1.0$ m.

[21] Another question which needs to be addressed when modelling the morphodynamic evolution of tidal networks is that, contrary to what happens in fluvial settings, tidal channels have a nonnegligible size with respect to the size of the system. Indeed, channeled areas make up a substantial part of the total tidal basin area. Moreover, tidal channel width contains crucial geomorphic information about the magnitude of landscape-forming flow rates shaping its cross sections. We therefore introduce a physically based criterion to assign the width of a tidal incision. To this end, we assume that the average channel depth, D, is related to the channel width, B, through the inverse of the width-to-depth ratio, β, which summarizes the complex morphodynamic mechanisms leading to an equilibrium cross section (e.g., see the review paper by *Darby* [1998] for alluvial channels and *Fagherazzi and Furbish* [2001] for the case of tidal creeks). In accordance with the observational evidence emerging from analyses of the geomorphic features of tidal networks discussed in section 2, we further assume that the cross-sectional area $\Omega(= B^2/\beta)$ is proportional to the drainage area, A, raised to an exponent α_A which varies in a neighborhood of 1. Our set of assumptions allows one to express Jarrett's "law," in the form $B \propto \sqrt{\beta A^{\alpha_A}}$, as a statement of instantaneous adaptation of the channel network to the hydrodynamic flow field and hence to the landscape-forming flow rates shaping its cross sections, at any stage of network evolution. This quite instantaneous adaptation to the hydrodynamic forcings is indirectly confirmed by approximately constant ratios of channel width,

B, to the radii of curvature in tidal meanders, i.e., in contexts where B changes spatially by orders of magnitude [*Marani et al.*, 2002]. The general effect of an increase in drainage area, considered as a surrogate of the landforming discharges, must be that of expanding channel cross-sectional areas. This postulates, as seen above and analogous to a number of models of salt marsh development [*Pethick*, 1969; *French and Stoddart*, 1992; *French*, 1993; *Allen*, 1997; *Steel and Pye*, 1997], the instantaneous adaptation of channel cross section, even if a time lag should be expected, in order to accommodate the swelling discharge shaping the channels. The effect of a decline in drainage area is similarly assumed to be a reduction of channel cross sections. Whether or not a decline should correspondingly reduce either channel width or depth or both, we leave to further developments.

[22] Summarizing the evidence and the hypotheses so far introduced, we assume that the mechanism dominating channel network development is its headward growth controlled by the exceedances of a critical shear stress, τ_c, which we take to coincide with a stability shear stress required to maintain an incised cross section through repeated tidal cycles. Whenever the local bottom shear stress, $\tau(\mathbf{x})$, exceeds τ_c anywhere on the border of the channels we expect erosional activity and network development. Channel width is calculated as a function of local drainage area as a surrogate of local landforming flow, postulating instantaneous adaptation of channel cross section to the hydrodynamic field.
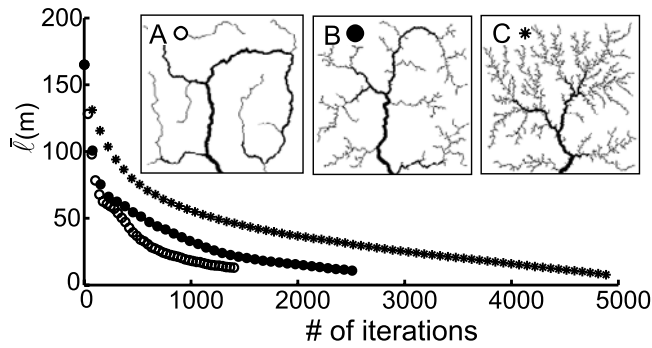
Figure 7. Evolution of the mean unchanneled length $\bar{\ell}$ as the network develops for the simulations A, B, and C represented in Figure 6.

[23] We expect heterogeneous geomorphological constraints to play a definite role in the development of tidal networks. Therefore in order to introduce the heterogeneity necessary to reproduce actual tidal networks, we assign the initial bottom elevation field, $z_b(\mathbf{x})$, as the sum of an average value, z_0, and an uncorrelated Gaussian noise, $z_1(\mathbf{x})$, which, owing to the assumptions embedded in equation (1) is chosen such that $z_1(\mathbf{x}) \ll \eta_0 - z_0$.

[24] Let us then consider a given tidal basin and let $\mathcal{S}$ be the current configuration representing one of the time steps of the network evolution process. As a consequence of network development, at a successive time step, the portion of the basin occupied by the channel network extends in space eroding the adjacent intertidal areas, $\Gamma_{\mathcal{S}}$, which on the contrary are subject to shrinking. The channels extend headward and branch in areas where the shear stress induced by the tidal flow, $\tau(\mathbf{x}; \mathcal{S})$, is greater than the threshold shear stress, τ_c. Depending on the spatial heterogeneity of sediment, vegetation and microphytobenthos, τ_c may be assumed as constant or space-dependent.

[25] To model the selective nature of the forces governing the evolution of the system, we introduce the analog of a simulated annealing procedure [Kirkpatrick et al., 1983]. This is an optimization technique which exploits an analogy with the way metals anneal when they are slowly cooled and thus atoms are allowed to arrange themselves into a crystalline structure with minimum free energy. In the framework of this similarity we choose changes from configuration $\mathcal{S}$ to configuration $\mathcal{S}'$ of the simulated network via a Boltzmann-like probability:

$$P(\mathcal{S}) \propto e^{-E(\mathcal{S})/T}, \qquad (4)$$

where T^{-1} is an analog of the Gibbs's parameter representing the inverse of temperature in classic thermodynamic systems and $E(\mathcal{S})$ is a measure of the energy of the system, which we assume to be represented by the average value of $\eta_1(\mathbf{x}; \mathcal{S})$ over the unchanneled portions of the tidal basin $\Gamma_{\mathcal{S}}$ (i.e., $E(\mathcal{S}) = \langle \eta_1(\mathbf{x}; \mathcal{S}) \rangle$). We shall use equation (4) to derive a rule for choosing among sites where thresholds are exceeded. The parameter T, by no means strictly a temperature in the thermodynamic sense, is seen as a proxy of the heterogeneity of the marsh substrate that allows the developing system to probe the number of possible

configurations of the final network that are characterized by the same mean potential energy: here the mean depth of the water surface over the datum surface. As such it controls the dynamic accessibility of steady state configurations.

[26] The Laplacian in equation (1) is estimated as a $L_1 \times L_2$ lattice discretization assuming an eight-neighbor scheme (four neighbors along the vertical and horizontal directions and four along the diagonals). For a given configuration $\mathcal{S}$, the evolution is performed according to the following rules.

[27] 1. Once the water surface $\eta_1(\mathbf{x}; \mathcal{S})$ has been determined by solving the Poisson boundary value problem (1), drainage directions, contributing areas to each pixel within the tidal basin, the energy of the system $E(\mathcal{S})$ and the probability $P(\mathcal{S})$ (equation (4)) are computed.

[28] 2. For each unchanneled site bordering the channel network the shear stress, $\tau(\mathbf{x}; \mathcal{S})$, is determined through equation (3). Threshold exceedances possibly scattered along the border of the channels, representing the sites where we expect activity, are computed and ranked.

[29] 3. A random value, R, uniformly distributed in $(0, 1)$ is drawn. If $R > P(\mathcal{S})$, the maximum (i.e., the first) exceedance $|\tau(\mathbf{x}; \mathcal{S}) - \tau_c|_{\max}$ is selected and that site becomes a part of the network, otherwise other random values $R^{(k)}$ are drawn (with $1 < k \leq N$, where N is the number of sites above threshold) until a $R^{(k)} > P(\mathcal{S})$ is found. The kth exceedance $|\tau(\mathbf{x}; \mathcal{S}) - \tau_c|_k$ is then selected (if $k > N$, one of the active sites is randomly chosen).

[30] 4. Once a newly connected pixel is found, the channel width, B, is computed on the basis of its contributing area and all the pixels which lie inside a circle centered on the newly connected pixel with a radius equal to $B/2$ become part of the network.

[31] 5. The network axis is outlined and the drainage area to any cross section is computed. An instantaneous adaptation of the network to the current flux shaping its cross section is performed. The configuration $\mathcal{S}'$ is therefore determined.

[32] Steps from 1 to 5 are repeated until no exceedance is found. Thus erosion processes cutting down the network come to an end when its structure has lowered the reference water surface elevations enough in the intertidal regions so
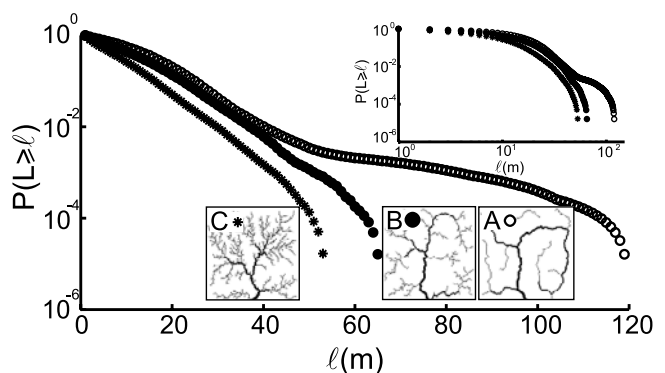

Figure 8. Semilog plot of the exceedance probability of unchanneled length $P(L \geq \ell)$ (versus the current value of length ℓ) computed for the final configurations of the experiments A, B, and C represented in Figure 6. The top inset shows the double logarithmic plot of the exceedance probability of unchanneled length $P(L \geq \ell)$.
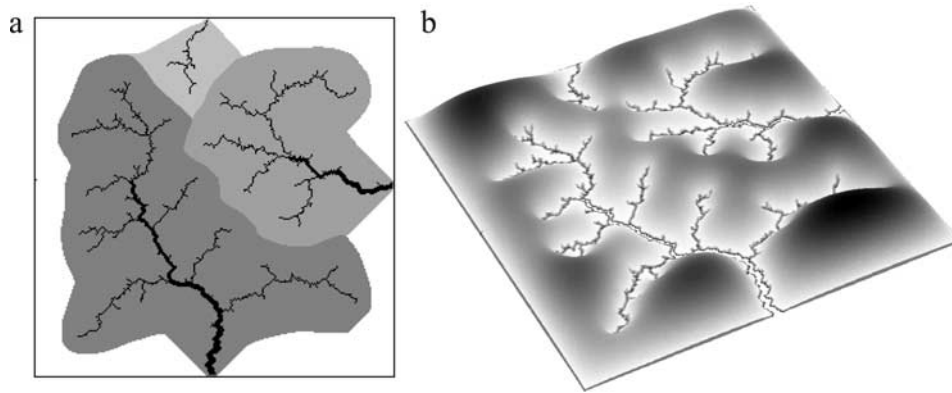
Figure 9. (a) Watershed delineation and planar configuration of channel networks developed by applying the model on a square domain Γ (to which a 256×256 lattice is superimposed) surrounded by channels on which the condition $\eta_1 = 0$ is applied. The painted areas represent the watersheds related to the inlets of the three channel networks, and the portion of the domain in white is drained by the surrounding channels. (b) Vertically exaggerated representation of the water surface elevation field $\eta_1(\mathbf{x}) = \eta_1(\mathbf{x}, \infty)$ derived by solving equation (1) in Γ. We have carried out this simulation by assuming $\tau_c = 0.3$ Pa, $T = 0.1$ m, $\beta = 6$, and $\alpha_A = 1.0$. The initial hydrodynamic conditions and the initial field of bottom elevations are the same as in Figure 5. See color version of this figure in the HTML.

that the threshold value of the shear stress, derived from the surface gradients, is nowhere exceeded.

4. Results

[33] We performed many experiments starting from different initial conditions in order to analyze the effects related to (1) the position of single or multiple inlets; (2) the shape of the tidal basin; (3) different initial conditions for the bottom topography $z_b(\mathbf{x})$; (4) different values of the width-to-depth ratio β and of the exponent α_A of the relationship $\Omega \propto A^{\alpha_A}$; and (5) different values of the critical shear stress for erosion τ_c and of the temperature T. In Figures 5 and 6 we show the final network configurations for some of the experiments carried out with a spatially constant value of the critical threshold τ_c. Figure 5 illustrates both the hydrodynamic potential used to infer flow directions and the resulting carved topography where channel walls appear smoothed, rather than vertical, due to the interpolation effect of the application. This series of results refers to network development within square, initially undissected tidal basins. No-flux boundary conditions are applied on all basins' boundaries. We assume that the inlet of the basin, located on the lower boundary representing a littoral barrier, is the result of a breach, e.g., by sea surges. This formation of a new opening in a narrow landmass, such as a barrier island or spit, allowing flows to be exchanged between a tidal embayment and the sea, is a common natural occurrence [e.g., *Bruun*, 1978]. On a smaller scale this setting may also represent the processes initiated by artificial breaching of levees in salt marsh restoration practices. According to our scheme, the pixel corresponding to the point where the breach occurs, on the seaward boundary of the domain, becomes a part of the network and it represents the initial channel network configuration $\mathcal{S}_0$. In particular, the networks of Figures 5 and 6 were obtained starting from the same hydrodynamic conditions and from the same initial conditions for the spatial distribution of bottom elevations (which we both

report in the caption of Figure 5). Figure 6 shows the effects of variations of the critical shear stress value, τ_c, and of the temperature, T, on network development. Because the position of the basin inlet is the same for all the simulations, the relevant characteristics of the flow field (i.e., $\eta_1(\mathbf{x}; \mathcal{S}_0)$, $\nabla \eta_1(\mathbf{x}; \mathcal{S}_0)$ and $\tau(\mathbf{x}; \mathcal{S}_0)$) at the first time step are the same. We observe (Figures 6a, 6b, and 6c) that, for a constant value of τ_c, different values of the temperature T lead to quite different final network configurations, per se an interesting result. A common behavior for the developing networks can be traced as follows. As the network moves from configuration $\mathcal{S}$ to $\mathcal{S}'$, via the erosion of those portions of the tidal basin in which exceedances of the threshold τ_c are found (and chosen), a general lowering of the water surface elevation $\eta_1(\mathbf{x}; \mathcal{S}')$ occurs. As a consequence, the average value of $\eta_1(\mathbf{x}; \mathcal{S}')$ over the flow field domain $\Gamma_{\mathcal{S}'}$ decreases. It directly follows that the energy of the system, $E(\mathcal{S}')$, that we
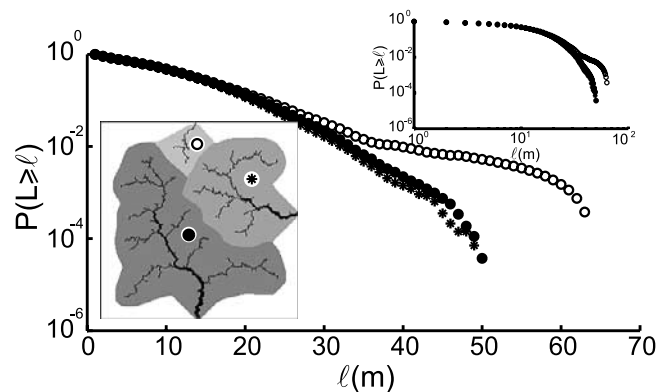

Figure 10. Semilog plot of the exceedance probability of unchanneled length $P(L \geq \ell)$ (versus the current value of length ℓ) computed for the three channel networks represented in Figure 9. The top inset shows the double logarithmic plot of the exceedance probability of unchanneled length $P(L \geq \ell)$.
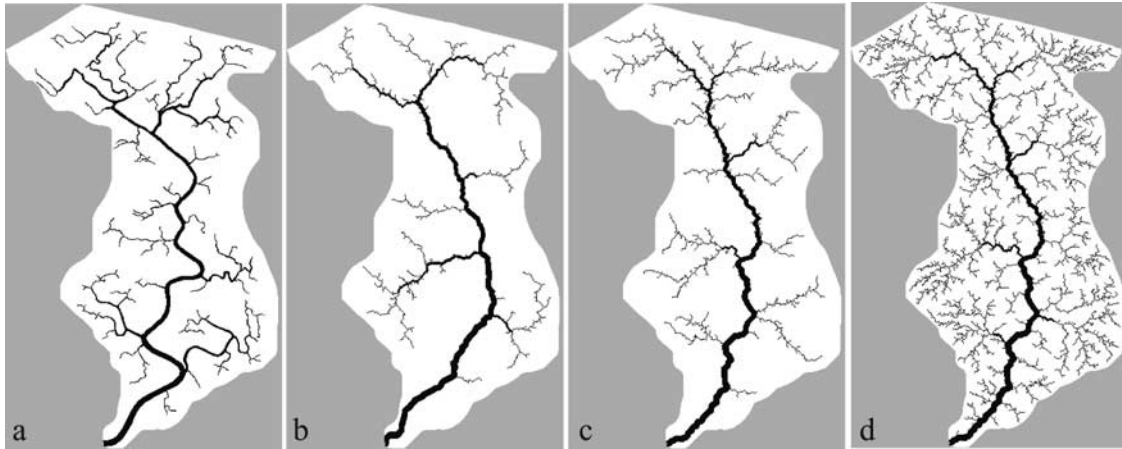
Figure 11. Comparison between (a) the planar configuration of an actual tidal network cutting through the Pagliaga salt marsh and (b–d) the planar configurations of synthetic networks obtained by applying the model on a domain represented by the real catchment for different values of τ_c and T. The initial hydrodynamic conditions are the same as in Figure 5. The initial field of bottom elevations $z_b(\mathbf{x}) = z_0 + z_1(\mathbf{x})$ was obtained by assuming $z_0 = 0$ m amsl and the uncorrelated Gaussian noise with mean $\langle z_1(\mathbf{x}) \rangle = 0$ and standard deviation $\sigma_{z_1(\mathbf{x})} = 0.02$ m. Other values of the parameters are $\beta = 6$ and $\alpha_A = 1.0$. (b) $\tau_c = 0.57$ Pa, $T = 0.1$ m; (c) $\tau_c = 0.57$ Pa, $T = 0.3$ m; (d) $\tau_c = 0.12$ Pa, $T = 0.3$ m.

assume to be measured by the average value of the water surface elevation over the domain (i.e., $E(\mathcal{S}') = \langle \eta_1(\mathbf{x}; \mathcal{S}') \rangle$), decreases. As a consequence, the probability $P(\mathcal{S}')$ increases (equation (4)). According to the simulated annealing procedure, during the initial stages of the evolution process, when the energy of the system $E(\mathcal{S}')$ is relatively high and the probability $P(\mathcal{S}')$ relatively low, the first random value R drawn is likely to be greater than $P(\mathcal{S}')$ and the maximum exceedance $|\tau(\mathbf{x}; \mathcal{S}') - \tau_c|_{max}$ is selected. Such being the case, the direction toward which erosion materializes is the direction of the greatest excess shear stress, which nearly coincides with the steepest descent direction for the water surface (equation (3)). Therefore during these initial stages, strong forces determined by the local gradient of surface elevation drive deterministically the erosion process and are actually responsible for network incision and maintenance. As the network develops, upon further lowering the field of free water surface elevations $\eta_1(\mathbf{x}; \mathcal{S}')$, the energy of the system $E(\mathcal{S}')$ decreases and the probability $P(\mathcal{S}')$ approaches 1. Other physical processes start then to contribute to network development and the direction of the maximum shear exceedance ceases to be the preferred direction for network growth. Low temperatures (Figures 6a and 6d) bear as a consequence very low values for the probability P and the point characterized by the largest shear stress is systematically selected during the process of network development. As the temperature T increases (Figures 6c and 6f), the lowering rate of the water surface $\eta_1(\mathbf{x})$ decreases and P approaches 1 faster. Figure 6a shows the deterministic network development resulting from the systematic choice of the maximum exceedances, which lowers the water surface $\eta_1(\mathbf{x})$, its gradients $\nabla\eta_1(\mathbf{x})$ and the values attained by the local shear stresses $\tau(\mathbf{x})$ in the fastest possible way. Values of P near to 1 are obtained later in the process of network development, and the direction toward which the network cuts down is likely to coincide with the direction characterized by greater values of the shear stress. As the temperature T grows, the increasingly stochastic character

of the synthetic networks (e.g., Figures 6c and 6f) mimics the occurrence of local heterogeneities that may affect network development.

[34] The number of time steps required to lower the water surface level until no exceedance of the threshold value, τ_c, is found, increases as the temperature, T, increases. In fact, in this case it becomes increasingly likely that a site with low exceedance is included in the network and the direction which would provide the fastest lowering of the free water surface is seldom selected. As a consequence, an increase in the degree of network incision is achieved for increasing temperature values and for a constant value of τ_c (e.g., Figures 6a, 6b, and 6c).

[35] Greater values of the critical threshold, τ_c, for a constant value of the temperature, T, (e.g., Figures 6a–6d, 6b–6e, and 6c–6f) lead to a decrease of the degree of channelization as a major effect, and possibly to different
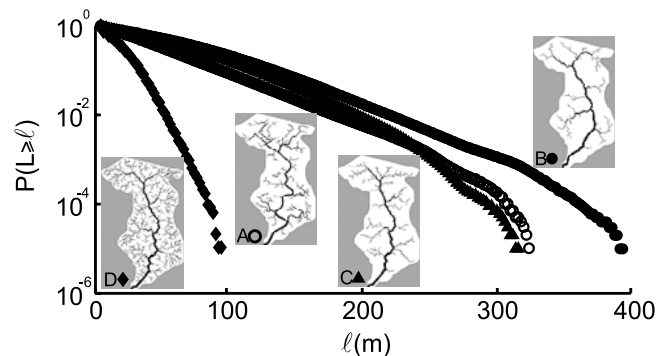

Figure 12. Comparison between the semilog plots of the exceedance probability of unchanneled length $P(L \geq \ell)$ (versus the current value of length ℓ) computed for the actual channel network cutting through the Pagliaga salt marsh and for the synthetic networks represented in Figure 11.
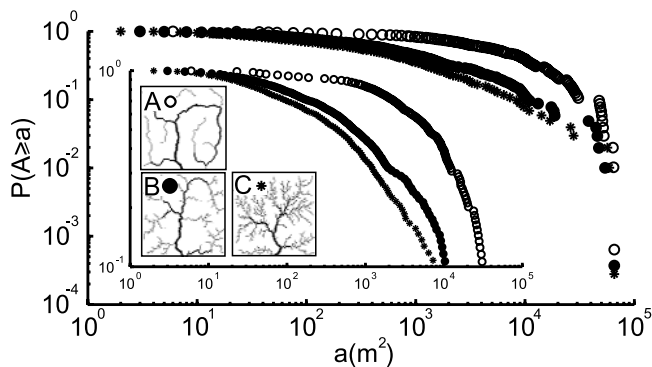
Figure 13. Double logarithmic plots of the exceedance probability of watershed area to any cross section of the network, $P(A \geq a)$ (versus the current value of area a) computed for the synthetic networks shown in Figures 6a, 6b, and 6c. The Inset shows a zoom of the upper range of probability ($10^{-1} \sim 10^{0}$).

structural organizations of the network. In fact, on one hand the degree of channelization decreases because greater values of τ_c imply that such threshold is nowhere exceeded earlier during the process of network development; on the other hand, network structure may undergo minor changes, due to the fact that a lower number of exceedances $|\tau(\mathbf{x}) - \tau_c|$, in which we expect activity, is found at any step of network development, and thus the choice of the pixel where erosion occurs embraces a smaller number of candidates.

[36] Figures 7 and 8 show the statistical properties of unchanneled flow lengths, ℓ, under different conditions, thus defining the drainage density of resulting tidal networks. Figure 7 shows the time evolution of the mean unchanneled length, $\bar{\ell}$, as the network develops through different planimetric configurations for the simulations A, B and C in Figure 6. Jointly with the intuitive result that $\bar{\ell}$ decreases as the network develops, it emerges that the lowering rate of $\bar{\ell}$ decreases as the temperature increases. This is a direct consequence of the fact that a decrease of the temperature, T, leads to larger lowering rates of the water surface, $\eta_1(\mathbf{x})$, and of the shear stress distribution, $\tau(\mathbf{x})$. The mean value of unchanneled lengths, $\bar{\ell}$, of the final configurations A, B and C decreases as the temperature increases, as seen in Figure 8, where semilog (and for comparison log-log) plots of the entire probability distributions (i.e., the cumulative probability of exceedance $P[L \geq \ell]$) for the networks in Figure 6 are shown. The approximately linear semilog trends suggest the type of exponential probability distributions observed for different tidal environments [*Marani et al.*, 2003].

[37] Figure 9 shows the result of a numerical experiment aimed at the study of competition for drainage and separate inlet formation. We carried out this experiment on a square domain in which the Poisson equation (1) was solved with the boundary condition $\eta_1 = 0$ on the outer boundary of the square domain, representing an island-like situation where intertidal areas are surrounded by deep tidal incisions. The initial inlet on the lower boundary was imposed at the beginning of the simulation but, quite interestingly, the other two inlets were automatically selected through the

evolution procedure described in section 3.2, thus underlining the capability of the model to capture important evolving features. In Figure 10 we show the semilog (and log-log) plots of the probability distributions of unchanneled lengths for the main watersheds outlined in Figure 9. The quite large lengths observed for the distribution pertaining to the smaller basin are related to the particular form of the (cusp-like) divides.

[38] We then performed a stringent test of the reliability of our modeling approach by simulating the development of a channel network within an actual catchment within one of our field sites [e.g., *Marani et al.*, 2003]. For this purpose, we considered a channel network within the Pagliaga salt marsh (Figure 1), determined its watershed via equation (1), computed the actual distribution of the shear stresses $\tau(\mathbf{x})$ (Figure 4) and imposed the rules of the model (section 3.2). The main results are shown in Figures 11 and 12. Notice that, just for visual purposes, we have selected the actual initial position of the inlet before letting the network cut down through the actual catchment watershed. In Figure 11 we compare the planimetric configuration of three synthetic networks (B, C, and D), obtained by varying the temperature T and τ_c, to the planimetric configuration of the observed network (A). Several interesting features emerge. In the simplest case (B), we have selected the maximum observed shear stress and imposed it as the threshold value; indeed, we expect the resulting network to yield a lower degree of network incision. While the model reproduces the major features of the actual tidal network, it cannot reproduce the complex structure resulting from tidal meandering, which are not taken into account here. Interestingly, the analysis of the probability distribution of unchanneled lengths ℓ (plot B of Figure 12) shows that the synthetic network exhibits an approximately linear trend in a semilog plot, suggesting the same type of exponential probability distribution exhibited by the actual network (Figure 2), though the mean length (which is the slope of the semilog plot) is higher as a result of the choice of the maximum threshold. Plot C of Figure 12 shows the same experiment run with the same threshold and a higher temperature, resulting in an increase in the degree of channelization and overall more realistic appearance. The mean unchan-
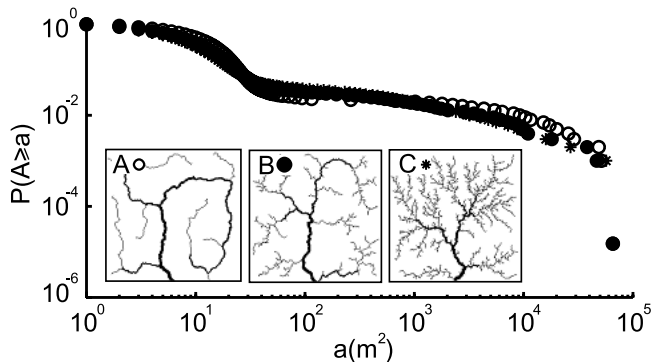

Figure 14. Double logarithmic plot of the exceedance probability of watershed area to any site within the tidal basin, $P(A \geq a)$ (versus the current value of area a) computed for the synthetic networks and their watersheds shown in Figures 6a, 6b, and 6c.
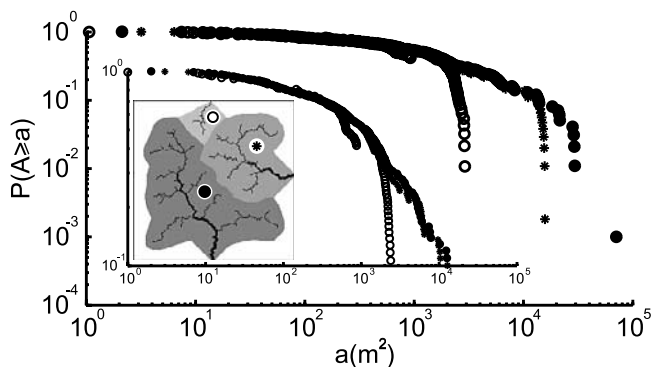
Figure 15. Double logarithmic plot of the exceedance probability of watershed area to any cross section, $P(A \geq a)$ (versus the current value of area a), computed for the three channel networks shown in Figure 9. The inset shows a zoom of the upper range of probability $(10^{-1} \sim 10^{0})$.

neled length matches (reasonably) that of the real marsh (plot A of Figure 12). Finally, Figure 11d shows the result of an experiment run using the lower threshold (corresponding to the mean of the observational distribution in Figure 4b), and the high temperature (as for Figure 11c). The mean unchanneled length is underestimated in this case, and the overall degree of channelization excessive. We thus conclude that the capabilities of the model to reproduce real-life features are noteworthy.

[39] Further analyses concerned another relevant geomorphic measure, namely, the exceedance probability of total contributing area, A, i.e., the fraction of sites (channeled or unchanneled) whose total contributing area exceeds a given value. Figures 13, 14, and 15 illustrate the log-log plots of the exceedance probability of watershed area, $P(A \geq a)$, for some of the networks and their watersheds shown in Figures 6 and 9. In particular, Figure 13 illustrates the exceedance probability of watershed area, A, to any cross section of the networks A, B and C of Figure 6. The non-power-law and rapidly decaying character of the exceedance probability emphasizes that the synthetic networks exhibit a lack of scale-invariant features in agreement with previous studies for observed networks developed in various tidal embayments [*Fagherazzi et al.*, 1999; *Rinaldo et al.*, 1999a, 1999b]. Figure 14 portrays the exceedance probability of watershed area, A, to any site within the tidal basins A, B and C of Figure 6. In this case the exceedance probability exhibits two distinct regimes, the first related unchanneled sites, characterized by small values of the drainage area, the second to channeled sites, with larger values of a. The non-power-law shape in the first regime indicates that also unchanneled sites exhibit a lack of scale-invariant features. Figure 15, which shows the exceedance probability of watershed area to any cross section of the three networks in Figure 9, makes it possible to extend the considerations developed for the networks of Figure 6 also to the island-like case of Figure 9.

[40] We then addressed the analysis of the spatial distribution of channel width, $B(s)$, as a function of the intrinsic channel axis coordinate, s, that is assumed to be positive in the landward direction. Tidal channels, in fact, quite often exhibit a nearly exponential landward decrease in width

[e.g., *Myrick and Leopold*, 1963; *Lanzoni and Seminara*, 2002; *Marani et al.*, 2002]. In order to describe such decrease, it is reasonable to assume a functional form of the type $B(s)/B_0 \sim \exp(-s/L_B)$, where B_0 is the initial channel width at $s = 0$, and L_B is the convergence length of the channel, estimated by a semilog linear fitting of B versus s. Figures 16 and 17 show the semilog plots of the ratio $B(s)/B_0$ versus s/L_B for some of our simulations in which the width-to-depth ratio, β, and the exponent, α_A, of the relationship $\Omega = 10^{-4}A^{\alpha_A}$ are varied. Networks developed within catchments with different boundary conditions have been analyzed (i.e., no-flux boundary conditions for Figure 16; $\eta_1 = 0$ on basins' boundaries for Figure 17). It is interesting to note (Figure 16) that although the seaward growth of $B(s)$ cannot be conclusively linked to an exponential trend as in some field sites [*Lanzoni and Seminara*, 2002; *Marani et al.*, 2002], it is reasonable to assume such a functional relationship. This is confirmed by the last experiment (Figure 17), where we have isolated two of the subbasins in Figure 9 which, differently from the previous case, have been selected by the internal dynamics of the system.

5. Conclusions

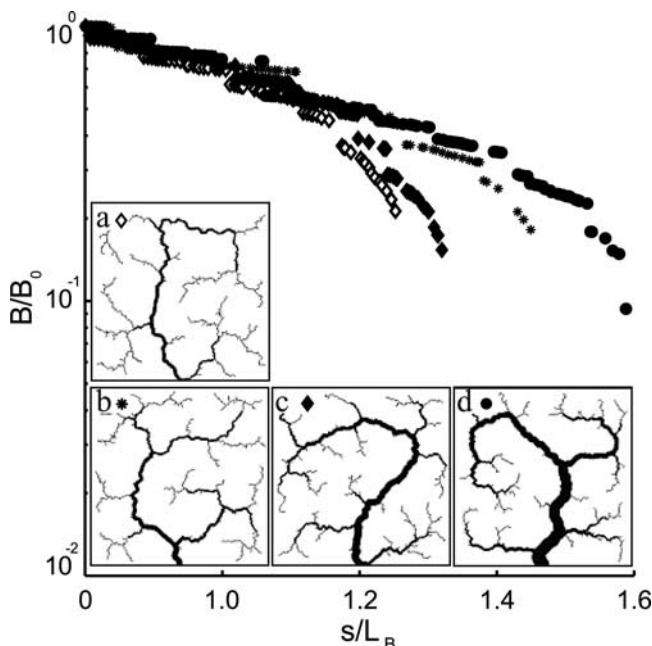[41] The main conclusions of this paper can be summarized as follows.

Figure 16. Logarithm of the ratio $B(s)/B_0$ versus s/L_B, where B_0 is the initial channel width at $s = 0$ and L_B is the convergence length, for different experiments obtained (in a square domain, to which a 256×256 lattice is superimposed) by varying the width-to-depth ratio β and the exponent α_A of the relationship $\Omega = 10^{-4}A^{\alpha_A}$. The width of the main channel in every experiment is dimensionless with its initial width. The initial hydrodynamic conditions and the initial field of bottom elevations are the same as in Figure 5. Other values of the parameters are $\tau_c = 0.3$ Pa and $T = 0.03$ m. (a) $\beta = 6$, $\alpha_A = 1.0$; (b) $\beta = 10$, $\alpha_A = 1.0$; (c) $\beta = 20$, $\alpha_A = 1.0$; (d) $\beta = 6$, $\alpha_A = 1.2$.
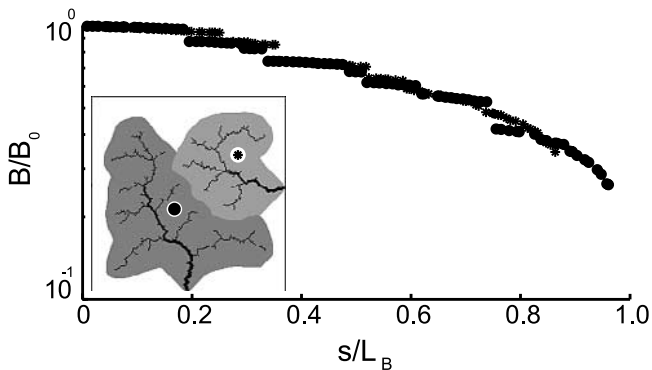
Figure 17. Logarithm of the ratio $B(s)/B_0$ versus s/L_B, where B_0 is the initial channel width at $s = 0$ and L_B is the convergence length, for two of the synthetic networks in Figure 9. The width of the main channel in every experiment is dimensionless with its initial width.

[42]   1. A model of tidal network ontogeny is proposed on the basis of a suitable hydrodynamic model which provides both flow directions and the field of shear stresses resulting from the requirements of channel formation, maintenance and spatial organization.

[43]   2. Field evidence supports the main assumptions, chiefly: the landscape-forming role of time-averaged free surfaces; the existence and consistency of width-to-depth ratios within channeled portions of the tidal landscape; the existence of a consistent and deterministic relationship between any channeled cross-sectional area and its embedded tidal prism (which we identify properly); the existence of a distribution of shear stresses representative of the conditions leading to channel formation and maintenance thereby mimicking the net balance of sediment production and transport.

[44]   3. The headward growth character of network development is supported by the spatial distribution of bottom shear stress computed via the simplified hydrodynamic model, displaying local maxima near channel tips.

[45]   4. The model proves reliable in reproducing several observed characteristics of geomorphic relevance (like length and area distributions), and capable of providing complex structures.

[46]   5. The model is designed to directly incorporate other key mechanisms operating over longer timescales, which have, in this first work, been neglected. Ecogeomorphic processes explicitly not included in the model presented, may nevertheless be described within the proposed framework in a relatively straightforward way. In particular, the vertical movement of intertidal areas can be modelled by introducing a suitable model of sedimentation, erosion and subsidence. This will also allow us to describe the evolution of the channel network in response to changes in the tidal prism due to variations in the elevation of tidal flats and salt marshes or in relative mean sea level. The influence of the vegetation distribution as well as of marine transgressions and regressions on channel network dynamics may, for example, be accounted for through a suitably time- and space-dependent τ_c. Tidal meandering may also be included, through use of established meander-

ing models, thus indicating that the work presented is a first step toward a comprehensive ecomorphological model of tidal environments.

References

Adam, P. (1990), *Salt Marsh Ecology*, Cambridge Univ. Press, New York.

Allen, J. R. L. (1990), Salt-marsh growth and stratification: A numerical model with special reference to the Severn Estuary, southwest Britain, *Mar. Geol.*, 95, 77–96.

Allen, J. R. L. (1995), Salt-marsh growth and fluctuating sea level: Implications of a simulation model for Flandrian coastal stratigraphy and peat-based sea-level curves, *Sediment. Geol.*, 100, 21–45.

Allen, J. R. L. (1997), Simulation models of salt-marsh morphodynamics: Some implications for high-intertidal sediment couplets related to sea-level change, *Sediment. Geol.*, 113, 211–223.

Allen, J. R. L. (2000), Morphodynamics of Holocene salt marshes: A review sketch from the Atlantic and southern North Sea coasts of Europe, *Quat. Sci. Rev.*, 19, 1155–1231.

Beeftink, W. G. (1966), Vegetation and habitat of the salt marshes and beach plains in the south-western part of The Nederlands, *Wentia*, 15, 83–108.

Boon, J. D. (1975), Tidal discharge asymmetry in a salt marsh drainage system, *Limnol. Oceanogr.*, 20, 71–80.

Boon, J. D., and R. J. Byrne (1981), On basin hypsometry and the morphodynamic response of coastal inlet systems, *Mar. Geol.*, 40, 27–48.

Bruun, P. (1978), *Stability of Tidal Inlets*, Elsevier, New York.

Callaway, J. C., J. A. Nyman, and R. D. DeLaune (1996), Sediment accretion in coastal wetlands: A review and a simulation model of processes, *Curr. Top. Wetland Biogeochem.*, 2, 2–23.

Christiansen, T., P. L. Wiberg, and T. G. Milligan (2000), Flow and sediment transport on a tidal salt marsh surface, *Estuarine Coastal Shelf Sci.*, 50, 315–331.

Collins, L. M., J. N. Collins, and L. B. Leopold (1987), Geomorphic processes of an estuarine marsh: Preliminary results and hypotheses, in *International Geomorphology 1986*, part I, edited by V. Gardner, pp. 1049–1072, John Wiley, Hoboken, N. J.

Darby, S. E. (1998), Modelling width adjustment in straight alluvial channels, *Hydrol. Processes*, 12, 1299–1321.

Di Silvio, G., and L. Dal Monte (2003), Ratio between channel cross-section and tidal prism in short lagoons: Validity and limits of the "Law of Jarrett," in *3rd IAHR Symposium on River, Coastal and Estuarine Morphodynamics, Barcelona, Spain*, vol. 1, pp. 524–533, Int. Assoc. for Hydraul. Res., Delft, Netherlands.

Fagherazzi, S., and D. J. Furbish (2001), On the shape and widening of salt marsh creeks, *J. Geophys. Res.*, 106, 991–1003.

Fagherazzi, S., A. Bortoluzzi, W. E. Dietrich, A. Adami, S. Lanzoni, M. Marani, and A. Rinaldo (1999), Tidal networks: 1. Automatic network extraction and preliminary scaling features from digital terrain maps, *Water Resour. Res.*, 35, 3891–3904.

Fagherazzi, S., P. L. Wiberg, and A. D. Howard (2003), Tidal flow field in a small basin, *J. Geophys. Res.*, 108(C3), 3071, doi:10.1029/2002JC001340.

French, J. R. (1993), Numerical simulation of vertical marsh growth and adjustment to accelerated sea-level rise, north Norfolk, U.K., *Earth Surf. Processes Landforms*, 81, 63–81.

French, J. R., and T. Spencer (1993), Dynamics of sedimentation in a tide-dominated backbarrier salt marsh, Norfolk, U.K., *Mar. Geol.*, 110, 315–331.

French, J. R., and D. R. Stoddart (1992), Hydrodynamics of salt marsh creek systems: Implications for marsh morphological development and material exchange, *Earth Surf. Processes Landforms*, 17, 235–252.

Friedrichs, C. T. (1995), Stability shear stress and equilibrium cross-sectional geometry of sheltered tidal channels, *J. Coastal Res.*, 11, 1062–1074.

Friedrichs, C. T., and D. G. Aubrey (1988), Non-linear tidal distortion in shallow weel-mixed estuaries: A synthesis, *Estuarine Coastal Shelf Sci.*, 27, 521–545.

Friedrichs, C. T., and J. E. Perry (2001), Tidal salt marsh morphodynamics, *J. Coastal Res.*, 27, 6–36.

Friedrichs, C. T., B. D. Armbrust, and H. E. de Swart (1998), Hydrodynamics and equilibrium sediment dynamics of shallow funnel-shaped tidal estuaries, in *Physics of Estuaries and Coastal Seas*, edited by J. Dronkers and M. Scheffers, pp. 315–327, A. A. Balkema, Brookfield, Vt.

Howard, A. D. (1994), A detachment-limited model of drainage basin evolution, *Water Resour. Res.*, *30*, 2261–2285.

Jarrett, J. T. (1976), Tidal prism-inlet area relationships, *Gen. Invest. Tidal Inlets Rep. 3*, 32 pp., U.S. Army Coastal Eng. Res. Cent., Fort Belvoir, Va.

Kirchner, J. W. (1993), Statistical inevitability of Horton's laws and the apparent randomness of stream channel networks, *Geology*, *21*, 591–594.

Kirkpatrick, S., G. D. Gelatt, and M. P. Vecchi (1983), Optimization by simulated annealing, *Science*, *220*, 671–680.

Lanzoni, S., and G. Seminara (1998), On tide propagation in convergent estuaries, *J. Geophys. Res.*, *103*, 30,793–30,812.

Lanzoni, S., and G. Seminara (2002), Long-term evolution and morphodynamic equilibrium of tidal channels, *J. Geophys. Res.*, *107*(C1), 3001, doi:10.1029/2000JC000468.

Lawrence, D. S. L., J. R. L. Allen, and G. M. Havelock (2004), Salt marsh morphodynamics: An investigation on tidal flows and marsh channel equilibrium, *J. Coastal Res.*, *20*, 301–316.

Leonard, L. A., and M. E. Luther (1995), Flow hydrodynamics in tidal marsh canopies, *Limnol. Oceanogr.*, *40*, 1474–1484.

Leopold, L. B., M. G. Wolman, and J. P. Miller (1964), *Fluvial Processes in Geomorphology*, W. H. Freeman, New York.

Leopold, L. B., J. N. Collins, and L. M. Collins (1993), Hydrology of some tidal channels in estuarine marshlands near San Francisco, *Catena*, *20*, 469–493.

Marani, M., S. Lanzoni, D. Zandolin, G. Seminara, and A. Rinaldo (2002), Tidal meanders, *Water Resour. Res.*, *38*(11), 1225, doi:10.1029/2001WR000404.

Marani, M., E. Belluco, A. D'Alpaos, A. Defina, S. Lanzoni, and A. Rinaldo (2003), On the drainage density of tidal networks, *Water Resour. Res.*, *39*(2), 1040, doi:10.1029/2001WR001051.

Marani, M., S. Lanzoni, S. Silvestri, and A. Rinaldo (2004), Tidal landforms, patterns of halophytic vegetation and the fate of the lagoon of Venice, *J. Mar. Syst.*, *51*, 191–210, doi:10.1016/j.jmarsys.2004.05.012.

Montgomery, D. R., and W. E. Dietrich (1988), Where do channels begin?, *Nature*, *336*, 232–234.

Myrick, R. M., and L. B. Leopold (1963), Hydraulics geometry of a small tidal estuary, *U.S. Geol. Surv. Prof. Pap.*, *422-B*, 18 pp.

Nichols, M. M., G. H. Johnson, and P. C. Peebles (1991), Modern sediments and facies model for a microcoastal plain estuary, the James estuary, Virginia, *J. Sediment. Petrol.*, *61*, 883–899.

O'Brien, M. P. (1969), Equilibrium flow areas of inlets in sandy coasts, *J. Waterw. Harbors Coastal Eng. Div. Am. Soc. Civ. Eng.*, *95*, 43–52.

Perillo, G. M. E. (1995), *Geomorphology and Sedimentology of Estuaries*, Elsevier, New York.

Pestrong, R. (1965), The development of drainage patterns on tidal marshes, *Publ. Geol. Sci. Tech. Rep. 10*, 87 pp., Stanford Univ., Stanford, Calif.

Pestrong, R. (1972), Tidal-flat sedimentation at Cooley Landing, southwest San Francisco Bay, *Sediment. Geol.*, *8*, 251–288.

Pethick, J. S. (1969), Drainage in tidal marshes, in *The Coastline of England and Wales*, 3rd ed., edited by J. R. Steers, pp. 725–730, Cambridge Univ. Press, New York.

Pethick, J. S. (1980), Velocity surges and asymmetry in tidal channels, *Estuarine Coastal Mar. Sci.*, *11*, 331–345.

Rigon, R., A. Rinaldo, and I. Rodríguez-Iturbe (1994), On landscape self-organization, *J. Geophys. Res.*, *99*, 11,971–11,993.

Rinaldo, A., and I. Rodríguez-Iturbe (1998), Channel networks, *Annu. Rev. Earth Planet. Sci.*, *26*, 289–327.

Rinaldo, A., I. Rodríguez-Iturbe, R. Rigon, R. L. Bras, and E. Ijjasz-Vasquez (1993), Self-organized fractal river networks, *Phys. Rev. Lett.*, *70*, 1222–1226.

Rinaldo, A., W. E. Dietrich, G. Vogel, R. Rigon, and I. Rodríguez-Iturbe (1995), Geomorphological signatures of varying climate, *Nature*, *374*, 632–636.

Rinaldo, A., S. Fagherazzi, S. Lanzoni, M. Marani, and W. E. Dietrich (1999a), Tidal networks: 2. Watershed delineation and comparative network morphology, *Water Resour. Res.*, *35*, 3905–3917.

Rinaldo, A., S. Fagherazzi, S. Lanzoni, M. Marani, and W. E. Dietrich (1999b), Tidal networks: 3. Landscape-forming discharges and studies in empirical geomorphic relationships, *Water Resour. Res.*, *35*, 3919–3929.

Rodríguez-Iturbe, I., and A. Rinaldo (1997), *Fractal River Basins: Chance and Self-Organization*, Cambridge Univ. Press, New York.

Rybczyk, J. M., J. C. Callaway, and J. W. Day (1998), A relative elevation model (REM) for a subsiding coastal forested wetland receiving wastewater effluents, *Ecol. Modell.*, *112*, 23–44.

Savenije, H. H. G. (2001), A simple analytical expression to describe tidal damping or amplification, *J. Hydrol.*, *243*, 205–215.

Schuttelaars, H. M., and H. E. de Swart (1996), An idealized long-term morphodynamic model of a tidal embayment, *Eur. J. Mech. B Fluids*, *15*, 55–80.

Schuttelaars, H. M., and H. E. de Swart (2000), Multiple morphodynamic equilibria in tidal embayments, *J. Geophys. Res.*, *105*, 24,105–24,118.

Silvestri, S., and M. Marani (2004), Salt marsh vegetation and morphology, modelling and remote sensing observations, in *The Ecogeomorphology of Tidal Marshes*, *Coastal Estuarine Stud.*, vol. 59, edited by S. Fagherazzi, M. Marani, and L. K. Blum, pp. 5–26, AGU, Washington, D. C.

Solari, L., G. Seminara, S. Lanzoni, M. Marani, and A. Rinaldo (2002), Sand bars in tidal channels. Part 2: Tidal meanders, *J. Fluid Mech.*, *451*, 203–238.

Speer, P. E., and D. G. Aubrey (1985), A study on non-linear tidal propagation in shallow inlet/estuarine systems, part II, Theory, *Estuarine Coastal Shelf Sci.*, *21*, 206–240.

Steel, T. J., and K. Pye (1997), The development of salt marsh tidal creek networks: Evidence from the UK, paper presented at the Canadian Coastal Conference, Can. Coastal Sci. and Eng. Assoc., Guelph, Ontario.

Stoddart, D. R., D. J. Reed, and J. R. French (1989), Understanding salt-marsh accretion: Scolt Head Island, Norfolk, England, *Estuaries*, *12*, 228–236.

van Dongeren, A. R., and H. J. de Vriend (1994), A model of morphological behaviour of tidal basins, *Coastal Eng.*, *22*, 287–310.

Ward, L. G., M. S. Kearney, and J. C. Stevenson (1998), Variations in sedimentary environments and accretionary patterns in estuarine marshes undergoing rapid submergence, Chesapeake Bay, *Mar. Geol.*, *151*, 111–134.

Yallop, M. C., B. de Winder, D. M. Paterson, and L. J. Stal (1994), Comparative structure, primary production and biogenic stabilisation of cohesive and non-cohesive marine sediments inhabited by microphytobenthos, *Estuarine Coastal Shelf Sci.*, *39*, 565–582.

————————————

A. D'Alpaos, S. Lanzoni, M. Marani, and A. Rinaldo, Dipartimento di Ingegneria Idraulica, Marittima Ambientale e Geotecnica, Università di Padova, via Loredan 20, I-35131 Padova, Italy. (adalpaos@idra.unipd.it; lanzo@idra.unipd.it; marani@idra.unipd.it; rinaldo@idra.unipd.it)

S. Fagherazzi, School of Computational Science and Information Technology Florida State University, Dirac Science Library, Tallahassee, FL 32306-4120, USA. (sergio@csit.fsu.edu)